# Insights into the Ultrafast Photodissociation Dynamics of Isoprene Derived Criegee Intermediates

Ernest Antwi, Niamh A. Packer, Jordyn M. Ratliff,[#] Barbara Marchetti, and Tolga N. V. Karsili*

*University of Louisiana at Lafayette, Lafayette, Louisiana, 70503, USA*

*Corresponding author contact details: tolga.karsili@louisiana.edu

[#]Author contributed as an undergraduate research assistant

**Abstract**

Isoprene is the most abundant non-methane volatile organic compound emitted into the troposphere by terrestrial vegetation. Reaction with ozone represents an important isoprene removal process from the troposphere and is a well-known source of Criegee intermediates (CIs), which are reactive carbonyl oxides. Three CIs, formaldehyde oxide ($CH_2OO$), methyl vinyl ketone oxide (MVK-oxide), and methacrolein oxide (MACR-oxide) are formed during isoprene ozonolysis. All three CIs contain strongly absorbing $\pi\pi^*$ states, electronic excitation to which leads to dissociation to form aldehyde/ketone + oxygen products. Here, we compare the excited state chemistry of $CH_2OO$, MVK-oxide and MACR-oxide in order to ascertain how increasing molecular complexity affects their photodynamics.

In $CH_2OO$, vertical excitation to the $S_2$ state leads to prompt O-O bond fission with a unity quantum yield. Branching into both the O ($^1$D) + $H_2CO$ ($S_0$) and O ($^3$P) + $H_2CO$ ($T_1$) product channels is predicted, with 80% of trajectories dissociating to form the former product pair. Analogous vertical excitation of the lowest energy conformers of MVK-oxide and MACR-oxide also undergoes O-O bond fission to form O + MVK/MACR products – albeit with a non-unity quantum yield. In the latter case, ca. 10% and 20 % of trajectories remain as the parent MVK-oxide and MACR-oxide molecule, respectively. Additionally, at most only 5% of the dissociating trajectories form O ($^3$P) + MVK/MACR ($T_1$) products, with a greater fraction forming O ($^1$D) + MVK/MACR ($S_0$) products (cf. $CH_2OO$). This latter observation coupled with the greater fraction of undissociated trajectories aligns with the bathochromic shift in the electronic absorption of the MACR-oxide and MVK-oxide (cf. $CH_2OO$). We discuss the

implications of the results in a broader context, including those that are relevant to the atmosphere.

## Introduction

Isoprene is the second most abundant volatile organic compound emitted into the troposphere by terrestrial vegetation. It has an annual emission rate of ca. 500 Tg $yr^{-1}$ and is particularly localized over deeply forested areas, such as the Amazon rainforest.(1, 2)

Reaction with the hydroxyl radical or ozone, represents two important sinks for the removal of isoprene from the troposphere. Reaction with ozone makes up 10% of the removal of isoprene and proceeds via a cycloaddition reaction of ozone across one of the two double bonds of the isoprene molecule, forming two distinct primary ozonides as shown in Fig. 1.(1) The resulting primary ozonide undergoes unimolecular decay to form ketone/aldehyde + carbonyl oxide products; the latter molecule is known as the Criegee intermediate (henceforth CI).

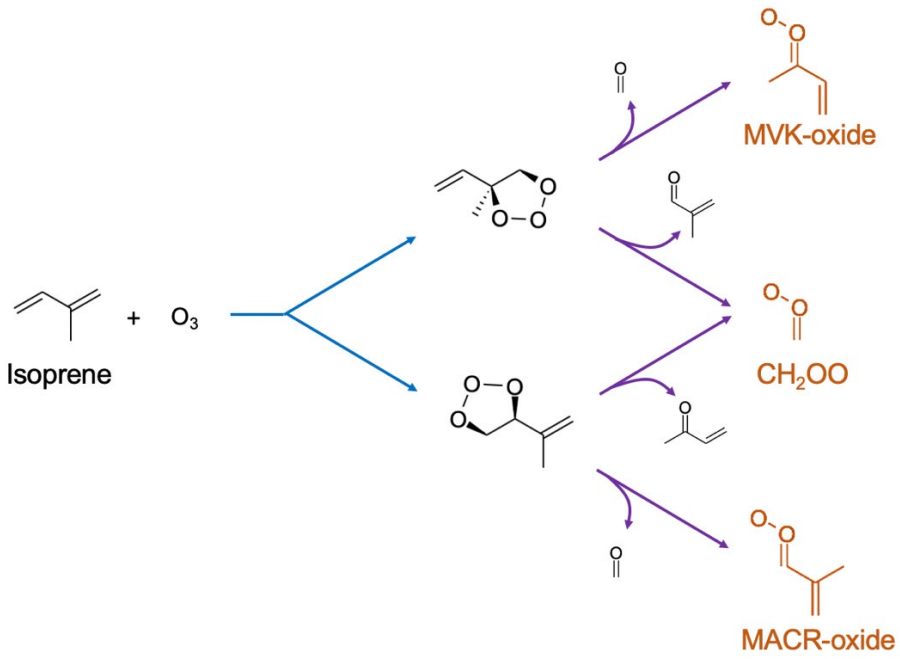

**Figure 1:** Ozonolysis reaction of isoprene for forming the three distinct CIs – formaldehyde oxide ($CH_2OO$), methyl vinyl ketone oxide (MVK-oxide) and methacrolein oxide (MACR-oxide). These CIs (displayed in orange) will be the focus on this study.

As Fig. 1 shows, isoprene ozonolysis proceeds via a [3+2]-cycloaddition of ozone across either one of two C=C double bonds of isoprene, forming two distinct primary ozonides. The nascent ozonides undergo unimolecular decay to form three distinct CIs – formaldehyde oxide ($CH_2OO$), methyl vinyl ketone oxide (MVK-oxide) and methacrolein oxide (MACR-oxide). The electronic absorption spectra of $CH_2OO$, MVK-oxide and MACR-oxide has attracted vast attention, from both an experimental(3–15) and computational(16–21) perspective. In all cases, the electronic absorption spectrum is dominated by a strongly absorbing $^1\pi\pi^*$ state, formed via an $\pi^* \longleftarrow \pi$ electron promotion. In $CH_2OO$, the onset of its electronic absorption is at ca. 420 nm, peaking at ca. 340 nm, and extending to ca. 280 nm.(4, 6, 22) Within this wavelength range, the tropospherically relevant solar actinic flux is minimal, with an average value of ca. $2 \times 10^{14}$ photons $cm^{-2}$ $s^{-1}$ $nm^{-1}$.(4) MVK-oxide and MACR-oxide represent an increase in molecular complexity (cf. $CH_2OO$) and have extended $\pi$-conjugation. As such, both molecules show a bathochromic shift in the electronic absorption profile relative to $CH_2OO$ which overlaps with the higher intensity edge of the tropospherically relevant solar actinic flux.(12, 15, 23) Additionally, the absolute absorption cross sections of both molecules are measured to be ca. 3-fold larger than $CH_2OO$.(15, 24) The associated bathochromic shift, coupled with the 3-fold increase in absorption cross section is expected to result in a higher solar photolysis rate for MVK-oxide and MACR-oxide (cf. $CH_2OO$) – potentially implicating solar photolysis as a tropospheric removal that is competitive with ground state unimolecular decay and bimolecular chemistry. While the latter two processes have been experimentally measured and theoretically characterized,(11, 25–29) the excited state dynamics of MVK-oxide and MACR-oxide has received comparatively little

attention. It should also be noted that the lowest energy conformers of MVK-oxide and MACR-oxide are long-lived under high-humidity conditions,(11, 27) implying that they may survive in the atmosphere and undergo photoexcitation.

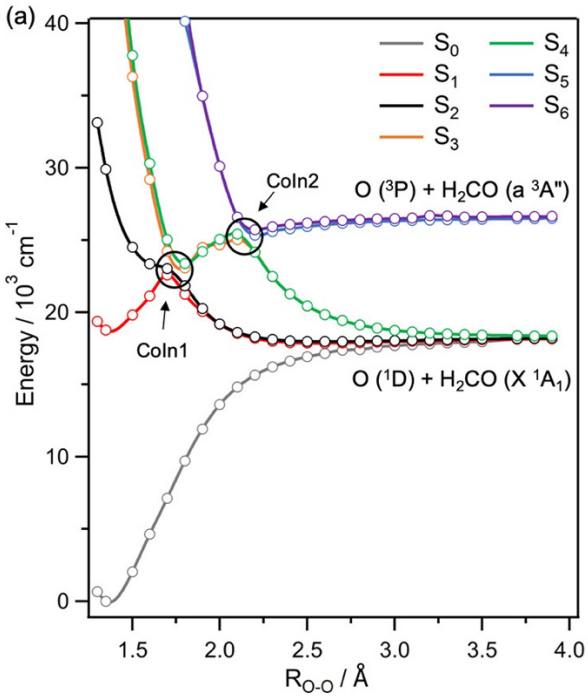


**Figure 2:** PE Profiles of the lowest seven electronic states of $CH_2OO$ along the O-O stretch coordinate. This figure is reproduced from reference (30).

Following electronic excitation, velocity map imaging (VMI) experiments have shown that $CH_2OO$, MVK-oxide and MACR-oxide undergo O-O bond fission, forming oxygen atom + carbonyl compound products.(22, 23, 30, 31) Upon excitation at $\lambda_{phot} \leq 350$ nm, $CH_2OO$ undergoes photodissociation to form two spin-allowed product channels corresponding to $H_2CO$ ($S_0$) + O ($^1D$) and $H_2CO$ ($T_1$) + O ($^3P$) products. Dissociation to form $H_2CO$ + O products can be understood by considering the potential energy (PE) profiles of $CH_2OO$ along the O-O stretch ($R_{OO}$) coordinate (reproduced in Fig. 2) – wherein the bright $S_2$ ($\pi\pi^*$) state is dissociative with respect to $R_{OO}$ and adiabatically correlates with the O ($^1D$) + $H_2CO$ ($S_0$) products. Our recent MS-

CASPT2 surface hopping study on $CH_2OO$ following vertical excitation to the $S_2$ ($^1\pi\pi^*$) state showed unity quantum yield for O-O bond fission – forming $H_2CO$ ($S_0$) + O ($^1D$) and $H_2CO$ ($T_1$) + O ($^3P$) products with an 80:20 branching in favor of the former products.(32) As Fig. 2 shows, formation of the higher energy $H_2CO$ ($T_1$) + O ($^3P$) product asymptote requires energies that are higher than that needed to populate the $S_2$ minimum energy geometry and involves internal conversion at two conical intersections (labeled Coln1 and CoIn2 in Fig. 2) located at $R_{OO} \sim 1.8$ Å and $R_{OO} \sim 2.2$ Å. These CoIns influence branching into the asymptotes corresponding to $H_2CO$ ($S_0$) + O ($^1D$) and $H_2CO$ ($T_1$) + O ($^3P$) products when nuclear motions traverse these regions of degeneracy. In addition, branching into the two asymptote channels may be influenced by CO stretch and HCO scissoring nuclear motions of the $H_2CO$ fragment that lead to degeneracies at asymptotic O-O bond distances.(32)

The topologies of the PE profiles along $R_{OO}$ in MVK-oxide and MACR-oxide mirror those of $CH_2OO$ (shown Fig. 2), with the exception that the $S_3$ state in MVK-oxide and MACR-oxide is bound at the Franck-Condon region.(23, 31) This latter observation is due to a second $^1\pi\pi^*$ state in MVK-oxide and MACR-oxide localized on the C=C moiety. This second $^1\pi\pi^*$ state has been experimentally and theoretically characterized for MVK-oxide and has its onsets of absorption that is well outside of the tropospherically relevant solar irradiance.(12, 23, 31) Following electronic excitation to the first $^1\pi\pi^*$ state of MVK-oxide and MACR-oxide, VMI experiments have measured O atom + methyl vinyl ketone (MVK) and O atom + methacrolein (MACR) products, respectively, indicating that both molecules also undergo O-O bond fission following electronic excitation to the bright $S_2$ state.(23, 31)

In this study we have undertaken a comparative computational study aimed at comparing the dynamics of $CH_2OO$, MVK-oxide and MACR-oxide following excitation to the bright $S_2$ state. In the latter two molecules, we focus only on the lowest energy conformer.

## Results and Discussion

The ground state minimum energy geometries of $CH_2OO$, *syn-trans*-MVK-oxide and *anti-trans*-MACR-oxide are displayed in Fig. 3. S*yn-trans* and *anti-trans* represent the lowest energy conformer of MVK-oxide and MACR-oxide, respectively. Although the structures (and conformer energies) of these molecules are now well-known,(12, 25) their description and depictions are important for the ensuing description of the dynamics.

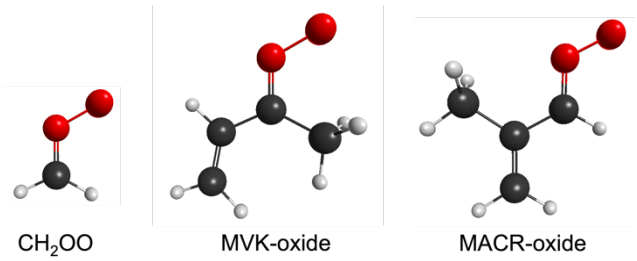


**Figure 3:** Ground state minimum energy structures of $CH_2OO$ (left), as well as the lowest energy – *syn-trans* and *anti-trans* – conformers of MVK-oxide and MACR-oxide, respectively.

In all cases, the ground state minimum energy geometry is with the C and O atoms in a common plane. MVK-oxide and MACR-oxide contain four conformers, distinguishable by rotation about the C=O and C=C bonds. Here we focus on the lowest energy *syn-trans* and *anti-trans* conformers of MVK-oxide and MACR-oxide, respectively. We note that the ozonolysis process will prepare the nascent MVK-oxide and MACR-oxide CIs with high internal energy, which may result in a non-equilibrium distribution of conformers. That said, experimental and computational studies have shown that their electronic absorption spectra are dominated by the

*syn*-MVK-oxide and *anti*-MACR-oxide conformers.(11, 33, 34) Moreover, we do not expect the photochemistry of the higher energy conformers to differ substantially from that of the lowest energy conformer.

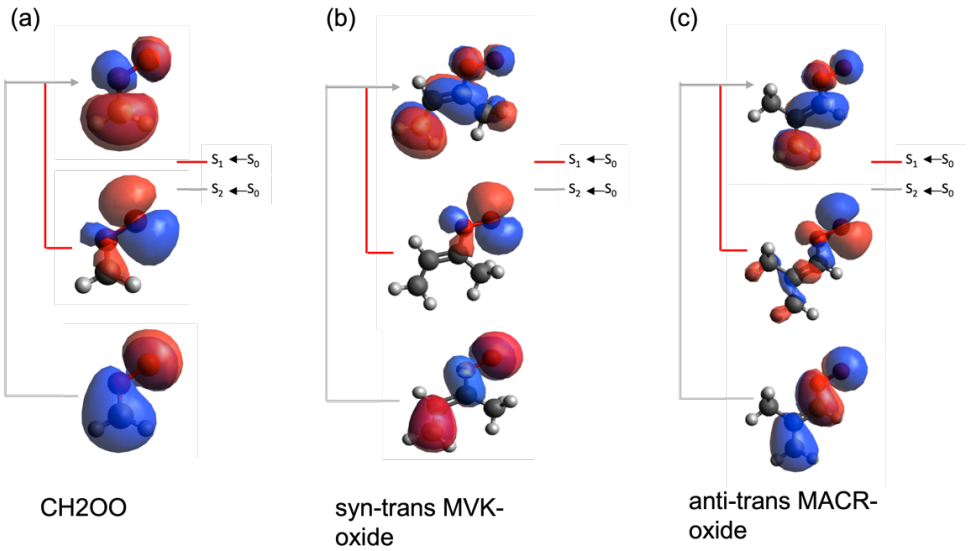


**Figure 4:** Orbitals and orbital promotions associated with the preparation of the $S_1$ and $S_2$ states of (a) $CH_2OO$, (b) *syn-trans*-MVK-oxide, and (c) *anti-trans*-MACR-oxide.

**Table 1:** Vertical excitation energies of the various CIs studied in the present study, calculated at the CASPT2/aug-cc-pVTZ level of theory. Minimum-to-minimum ($D_e$) and anharmonic zero-point corrected ($D_0$) bond dissociation energies of the two product channels are calculated at the CCSD(T)-F12b/cc-pVTZ-F12 level of theory.

| **Criegee intermediate** | **Vertical Excitation Energy ($^1\pi\pi^*$-$S_0$) / eV (nm)** | **O($^1$D) + R'R"CO ($S_0$) / eV** | | **O($^3$P) + R'R"CO ($T_1$) / eV** | |
|---|---|---|---|---|---|
| | | **$D_e$** | **$D_0$** | **$D_e$** | **$D_0$** |
| $CH_2OO$ | 3.91 (317) | 2.51 | 2.39 | 3.58 | 3.37 |
| MVK-oxide | 3.50 (355) | 2.74 | 2.65 | 3.74 | 3.56 |
| MACR-oxide | 3.29 (376) | 2.55 | 2.45 | 3.59 | 3.39 |

Fig. 4 presents the orbitals and orbital promotions associated with forming the $S_1$ and $S_2$ states of $CH_2OO$, MVK-oxide and MACR-oxide. Following vertical excitation, the $S_1$ and $S_2$ states in $CH_2OO$, MVK-oxide, and MACR-oxide are of $n\pi^*$ and $\pi\pi^*$ character, respectively. The former

$^1n\pi^*$ state is formed via an $\pi^* \leftarrow n$ electron promotion, wherein the participating orbitals show poor spatial overlap. This manifests in a weak absorption cross section for excitation to the $^1n\pi^*$ state. In contrast, the $S_2$ ($^1\pi\pi^*$) state is formed via a $\pi^* \leftarrow \pi$ electron promotion, wherein the participating orbitals show appreciable spatial overlap. This manifests in the characteristically high absorption cross section for excitation to the $^1\pi\pi^*$ state. As Table 1 shows, The $S_2 \leftarrow S_0$ vertical excitation energies of MVK-oxide and MACR-oxide are bathochromic with respect to the equivalent electronic transition in $CH_2OO$. This is a manifestation of the extended π-conjugations in MVK-oxide and MACR-oxide (cf. $CH_2OO$). The $S_2 \leftarrow S_0$ vertical excitation energies of MACR-oxide is bathochromic with respect to MVK-oxide, which is in excellent agreement with the experimentally measured electronic absorption spectrum of MVK-oxide and MACR-oxide. Upon electronic excitation to the $^1\pi\pi^*$ state, experiments conclude that $CH_2OO$, MVK-oxide and MACR-oxide undergo O-O bond fission.

At selected wavelengths, $CH_2OO$ forms both O ($^1D$) + $H_2CO$ ($S_0$) and O ($^3P$) + $H_2CO$ ($T_1$) products. As Fig. 2 demonstrates, the former set of products arise via dissociation on the $S_0$, $S_1$, $S_2$, $S_3$, $S_4$ and $S_5$ states, while the latter products arise via dissociation on the $S_6$ and $S_7$ states – which requires internal conversion at both CoIn1 and CoIn2. The correlation of these various states one or the two asymptotes may be understood by considering the electronic configurations of $S_0$-$S_6$ states at long $R_{OO}$, which is given in Fig. 5. As Fig. 5 shows, the electronic configurations of the $S_0$-$S_4$ states at long $R_{OO}$ are distinguishable by five distinct (but degenerate) arrangements of the 2p electrons that give rise to the $^1D$ electronic term of the departing O atom – indicating that the $S_0$-$S_4$ states converge to the same O ($^1D$) + $H_2CO$/MVK/MACR ($S_0$) limit. Similarly, the $S_5$ and $S_6$ states at long $R_{OO}$ are distinguishable by two distinct arrangements of the 2p electrons that return the $^3P$ electronic term of the terminal O atom. In addition, both $S_5$ and $S_6$

states show the $H_2CO$/MVK/MACR counter-fragment in its $T_1$ electronic configuration. As such, the $S_5$ and $S_6$ states converge to the same O ($^3P$) + $H_2CO$/MVK/MACR ($T_1$) limit.

In the case of $CH_2OO$, recent trajectory surface hopping studies have shown that the O ($^1D$) + $H_2CO$ ($S_0$) products are favored over the higher energy O ($^3P$) + $H_2CO$ ($T_1$) products. As Table 1 shows, the zero-point energy corrected ($D_0$) and non-zero-point energy corrected ($D_e$) bond dissociation energies for forming the O ($^1D$) + $H_2CO$/MVK/MACR ($S_0$) product channel is energetically accessible following vertical excitation to the $S_2$ state of $CH_2OO$/MVK-oxide/MACR-oxide. In $CH_2OO$, the $D_e$ and $D_0$ values for forming the O ($^3P$) + $H_2CO$ ($T_1$) products are also below the $S_2$ state vertical excitation energies, indicating that the higher energy asymptote is also accessible following vertical excitation to the $S_2$ state. In contrast, the $D_0$ and $D_e$ values associated with forming the O ($^3P$) + MVK ($T_1$) and O ($^3P$) + MACR ($T_1$) products are above the predicted $S_2$ vertical excitation energy of MVK-oxide and MACR-oxide, respectively.

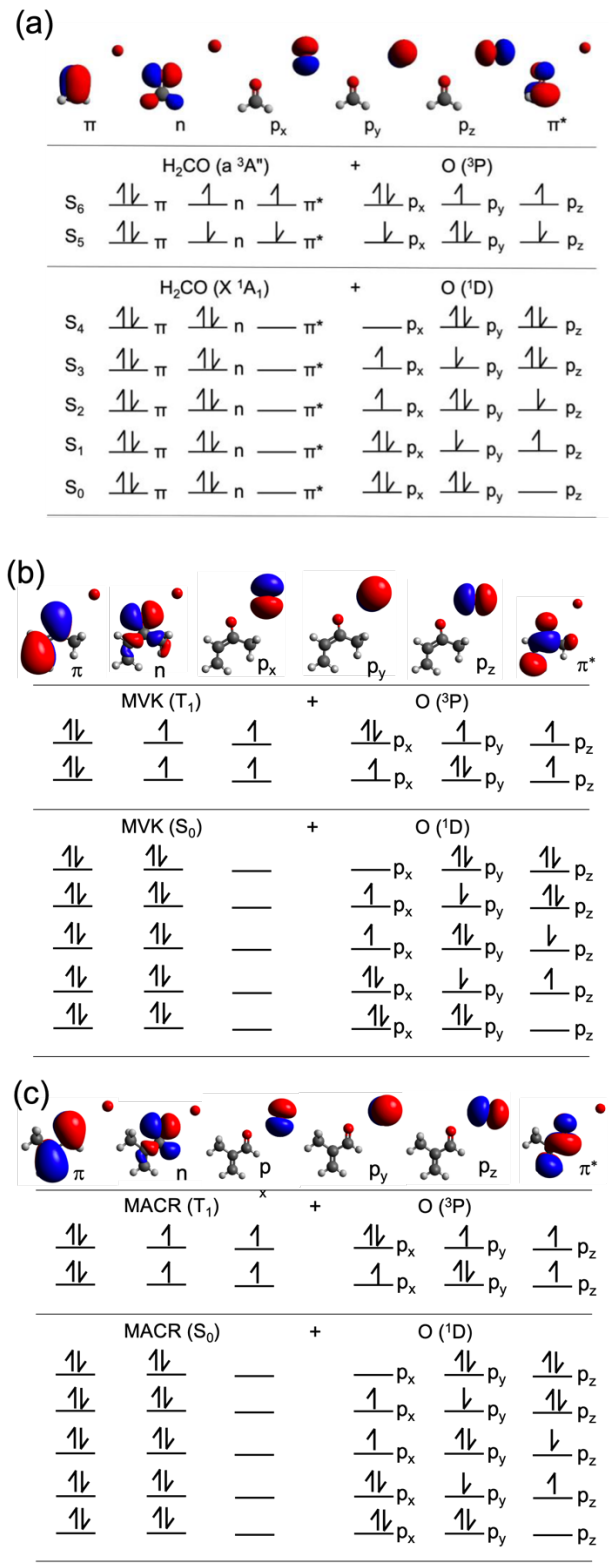


**Figure 5:** The electronic configurations associated with the seven electronic states of (a) $CH_2OO$, (b) MVK-oxide and (c) MACR-oxide, at long O-O distances corresponding to the two asymptotic product channels.

In order to characterize and compare the excited state dynamics of $CH_2OO$, MVK-oxide and MACR-oxide, we have undertaken MS-CASPT2 trajectory surface hopping (TSH) studies by vertically projecting the initially prepared trajectories to the $S_2$ state (see methodology section). Fig. 6 presents the normalized populations in the $S_0$, $S_1$, $S_2$, $S_3$, $S_4$, $S_5$ and $S_6$ states as a function of time for (a) $CH_2OO$, (b) *syn-trans*-MVK-oxide, and (c) *anti-trans*-MACR-oxide. The data associated with $CH_2OO$ are reproduced from reference (30). As Fig. 6(a) shows, the pre-excited $S_2$ state of $CH_2OO$ undergoes depopulation after ca. 10 fs – wherein ca. 80 % of the final population at 50 fs partitions across the $S_0$-$S_5$ states, while the remaining ca. 20% is distributed amongst the $S_5$ and $S_6$ state. As Fig. 7(a) shows, the fate of these trajectories following vertical excitation to the $S_2$ state is O-O bond elongation, thus leading to photodissociation to form O + $H_2CO$ products. This latter observation, coupled with the state populations at 50 fs, implies an electronic state branching ratio of 80:20 in the O ($^1D$) + $H_2CO$ ($S_0$) and O ($^3P$) + $H_2CO$ ($T_1$) products, respectively.

Figs. 6(b) and 6(c) present the variations in the $S_0$-$S_6$ population as a function of time for the more complex CIs, MVK-oxide and MACR-oxide. As these figures show, the $S_2$ state is depopulated slower than $CH_2OO$ with a substantially smaller fraction of the total population internally converting to the $S_5$ and $S_6$ states. This latter observation implies that the asymptotic limit for forming the O ($^3P$) + $H_2CO$ ($T_1$) products is less important in the cases of MVK-oxide and MACR-oxide (cf. $CH_2OO$). To check if a greater population undergoes internal conversion to the $S_5$ and $S_6$ states at later time, we continued our TSH simulations for MVK-oxide and MACR-oxide for an additional 50 fs, giving a total propagation time of 100 fs (see Fig S1 of the supporting information). As Fig. S1 shows, the population in the $S_5$ and $S_6$ states remain constant beyond 50 fs.

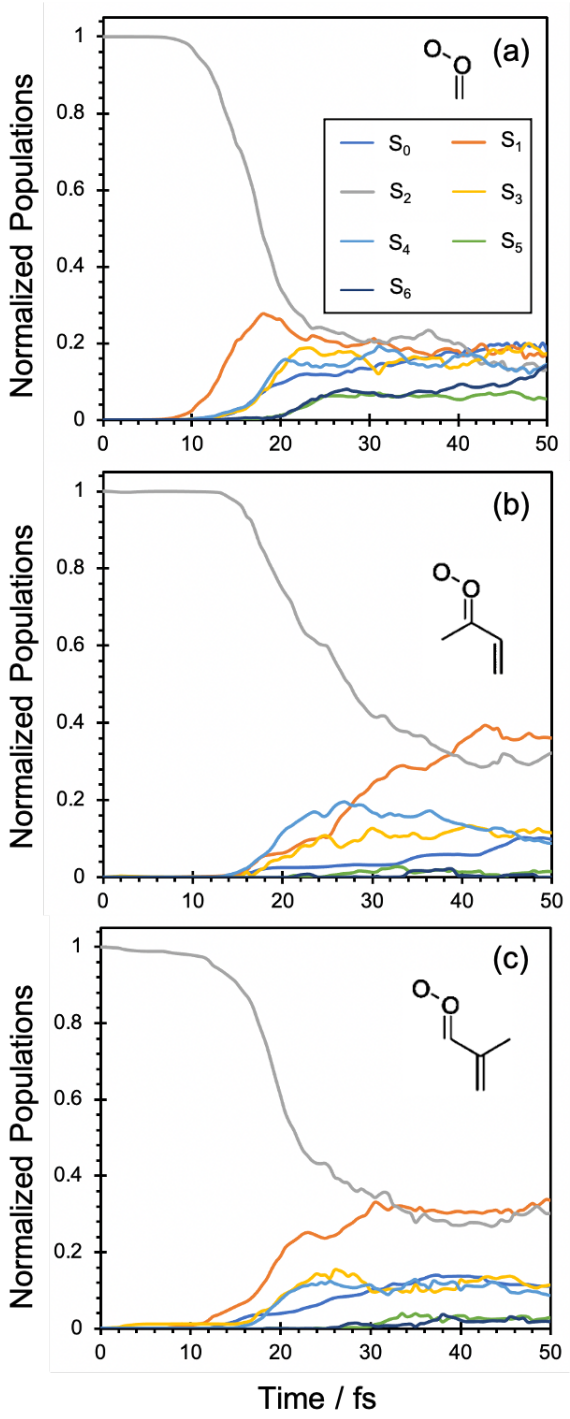


**Figure 6:** Populations as a function of time for (a) $CH_2OO$, and the lowest energy conformer of (b) MVK-oxide and (c) MACR-oxide.

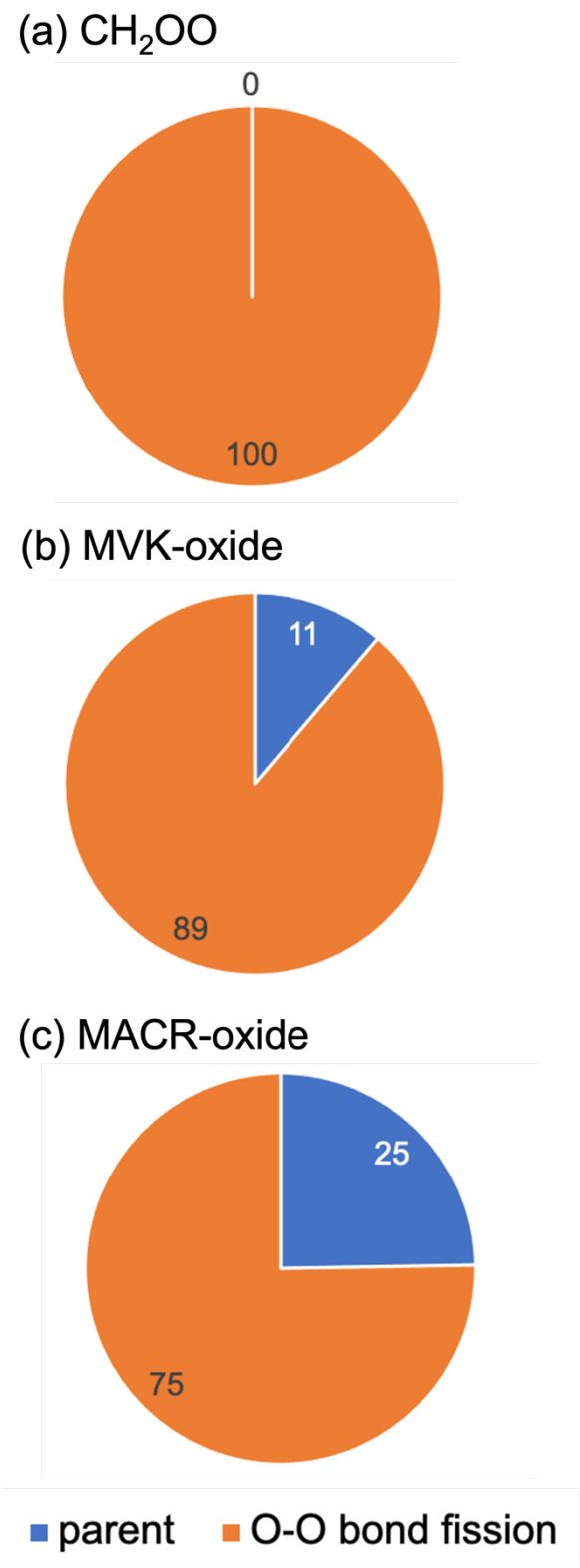


**Figure 7:** Fraction of trajectories that undergo O-O bond fission versus remain as parent molecules following excitation to the $S_2$ state.

Inspection of trajectories reveals that all $S_2$ vertically excited $CH_2OO$ trajectories undergo O-O bond fission to form O + $CH_2O$ products with unity quantum yield. As fig. 7 (a) and (b) shows, the $S_2$ vertically excited MVK-oxide and MACR-oxide molecules undergo O-O bond fission with non-unity quantum yields of 89% and 75%, respectively. The remaining quantum yield is partitioned in undissociated parent molecules in either the $S_2$ or the $S_1$ state (following internal conversion). This implies that fewer MVK-oxide and MACR-oxide trajectories contain the required energy to traverse regions beyond the $S_2$ Franck-Condon region and undergo dissociation to form O + MVK/MACR products (cf. $CH_2OO$). This latter statement is supported by the vertical excitation energies and bond dissociation energies listed in Table 1, which shows that the $S_2$ vertical excitation energies of MVK-oxide and MACR-oxide are bathochromic with respect to that of $CH_2OO$. This observation is due to the extended π-conjugation in MVK-oxide and MACR-oxide. In addition, while the bond dissociation energies of $CH_2OO$ and MACR-oxide are similar, those of MVK-oxide are ca. 0.15 eV higher than $CH_2OO$ and MACR-oxide. This can be understood by recognizing that the lowest energy *syn-trans* conformer of MVK-oxide is weakly hydrogen-bonded – between the methyl centered H-atom and the terminal oxygen atom. This weak hydrogen bonding affords additional stabilization for MVK-oxide and thus a higher bond dissociation energy for form O + MVK products. The stronger bond dissociation energy for MVK-oxide is however offset by the larger bathochromic shift in the $S_2$ absorption in MACR-oxide. As Table 1 shows, the energy difference between the $S_2$ VEE and the $D_e$ (for forming $O(^1D)$ + MVK/MACR ($S_0$) products) for MACR-oxide is less exothermic than that for MVK-oxide – which might support the observation that fewer trajectories dissociate in the case of MACR-oxide.

## Conclusions

In this article we have undertaken a MS-CASPT2 surface hopping study of the excited state dynamics of the isoprene derived CIs: $CH_2OO$, MVK-oxide and MACR-oxide, following vertical excitation to the $S_2$ state. Vertical excitation of $CH_2OO$ leads to O-O bond fission with unity quantum yield, and an 80:20 branching into the $H_2CO$ ($S_0$) + O ($^1D$) and $H_2CO$ ($T_1$) + O ($^3P$) product channels. Dissociation to form the analogous two asymptotic products is also observed in the case of photoexcited MVK-oxide and MACR-oxide – albeit with a non-unity quantum yield and a greater preference for forming MVK/MACR ($S_0$) + O ($^1D$) products.

The results highlight the variations in the photochemistry of a CI upon increasing molecular complexity, with the results of potential significance for larger CIs that are derived from carbene oxidation. Given the bathochromic shift in the electronic absorption, coupled with the increase absorption cross section, MVK-oxide and MACR-oxide are expected to have an enhanced photolysis rate compared to smaller CIs.(34) This may have implications on the tropospheric budget of O($^1D$), which is dominantly formed from the photodissociation of $O_3$. While we expect unimolecular decay to play a significant role in limiting the atmospheric lifetimes of MVK-oxide and MACR-oxide, we also note that the lower energy conformers of both are substantially longer-lived than $CH_2OO$.(35, 36) Moreover, the fraction of $S_2$ excited MVK-oxide and MACR-oxide that survives and remains as parent molecules may undergo internal conversion to the $S_1$ and $S_0$ states on longer timescales, as well as undergoing intersystem crossing to triplet states; the latter was deemed to be insignificant in our previous work on $CH_2OO$.(37)

Moving forward, we plan to extend this body of work by comparing the photochemistry of the present isoprene derived CIs to those derived from α-pinene ozonolysis, as well as those derived from carbene precursors that are relevant to synthetic chemistry.

## Computational Methodology

The ground state minimum energy geometry of *syn-trans*-MVK-oxide and *anti-trans*-MACR-oxide was optimized at the B2PLYP-D3/cc-pVTZ level of theory.(38, 39) This level of theory has been previously shown to perform well for determining geometries and normal modes wavenumbers of CIs.(20, 25, 30, 31) Its use also allows for consistency when comparing the present simulations with prior work.(30, 40) Trajectory surface hopping (TSH) simulations were performed using the Newton-X computational package.(41, 42) Initial positions and momenta were sampled using a Wigner distribution; these were based on the B2PLYP-D3/cc-pVTZ ground state minimum energy geometry and its associated harmonic normal mode wavenumbers. In the TSH simulations, the nuclear coordinates were propagated by integrating Newton's equation using the velocity Verlet method, while the electronic coordinates were propagated by numerically solving the time-dependent Schrödinger equation using Butcher's fifth-order Runge-Kutta method in steps of 0.025 fs.(43) Trajectories were initiated in the $S_2$ state and the energies and gradients of the seven lowest singlet states were calculated "on-the-fly" using the SS-SR-CASPT2 method in coupled with the cc-pVDZ basis set.(44) SS-SR-CASPT2 enables the computation of energies and analytical gradients at MS-CASPT2 quality, at a reduced computational cost; it also performs well near electronic state degeneracies. The SS-SR-CASPT2 calculations were based on a state-averaged complete active space self-consistent field (CASSCF) method reference wavefunction and an active space comprising 10 electrons in 8 orbitals as depicted in Fig. S2-S4 of the supporting information. These were performed via the BAGEL interface to Newton-X.(45) The state hopping probabilities were evaluated by calculating the non-adiabatic coupling matrix elements from the SS-SR-CASPT2 computations.

89 and 93 trajectories were propagated in time with a step size of 0.5 fs for MVK-oxide and MACR-oxide, respectively.

Additional calculation at the B2PLYP-D3/cc-pVTZ level of theory were carried out on the $H_2CO$, MVK and MACR counter-fragments formed via O-O bond fission of their starting parent molecule. Single-point energy calculates were performed on the resulting optimized structure of the $H_2CO$, MVK and MACR products, as well as the starting $CH_2OO$, MVK-oxide, and MACR-oxide, at the explicitly correlated CCSD(T)-F12b/cc-pVTZ-F12 level of theory. Vertical excitation energies of the B2PLYP-D3/cc-pVTZ optimized $CH_2OO$, MVK-oxide, and MACR-oxide molecules were calculated at the single-state CASPT2/aug-cc-pVTZ level of theory. The same 10/8 active space as the trajectory simulations was used in these latter CASPT2 calculations.

The CCSD(T)-F12b and CASPT2 calculations were performed using Molpro,(46, 47) while the Density Functional Theory computations were carried out using Gaussian 16.(48)

**Acknowledgements**

The work reported in this article is supported by the National Science Foundation, under grant no. 2003422. Portions of this research were conducted with high performance computational resources provided by the Louisiana Optical Network Infrastructure (http://www.loni.org).

**Reference**

1. Sindelarova, K., Granier, C., Bouarar, I., Guenther, A., Tilmes, S., Stavrakou, T., Müller, J. F., Kuhn, U., Stefani, P. and Knorr, W. (2014) Global data set of biogenic VOC emissions calculated by the MEGAN model over the last 30 years. *Atmos. Chem. Phys.* **14**, 9317–9341.

https://doi.org/10.5194/acp-14-9317-2014.

2. Nguyen, T. B., Tyndall, G. S., Crounse, J. D., Teng, A. P., Bates, K. H., Schwantes, R. H., Coggon, M. M., Zhang, L., Feiner, P., Milller, D. O., Skog, K. M., Rivera-Rios, J. C., Dorris, M., Olson, K. F., Koss, A., Wild, R. J., Brown, S. S., Goldstein, A. H., de Gouw, J. A., Brune, W. H., Keutsch, F. N., Seinfeld, J. H. and Wennberg, P. O. (2016) Atmospheric fates of Criegee intermediates in the ozonolysis of isoprene. *Phys. Chem. Chem. Phys.* **18**, 10241–10254. https://doi.org/10.1039/C6CP00053C.

3. Chang, Y. P., Li, Y. L., Liu, M. L., Ou, T. C. and Lin, J. J. M. (2018) Absolute Infrared Absorption Cross Section of the Simplest Criegee Intermediate Near 1285.7 cm-1. *J. Phys. Chem. A* **122**, 8874–8881. https://doi.org/10.1021/acs.jpca.8b06759.

4. Ting, W. L., Chen, Y. H., Chao, W., Smith, M. C. and Lin, J. J. M. (2014) The UV absorption spectrum of the simplest Criegee intermediate CH 2OO. *Phys. Chem. Chem. Phys.* **16**, 10438–10443. https://doi.org/10.1039/c4cp00877d.

5. Sheps, L., Scully, A. M. and Au, K. (2014) UV absorption probing of the conformer-dependent reactivity of a Criegee intermediate CH3CHOO. *Phys. Chem. Chem. Phys.* **16**, 26701–26706. https://doi.org/10.1039/C4CP04408H.

6. Sheps, L. (2013) Absolute Ultraviolet Absorption Spectrum of a Criegee Intermediate CH 2OO. *J. Phys. Chem. Lett.* **4**, 4201–4205. https://doi.org/10.1021/jz402191w.

7. Caravan, R. L., Vansco, M. F., Au, K., Khan, A. A. H., Li, Y. L., Winiberg, F. A. F., Zuraski, K., Lin, Y. H., Chao, W., Trongsiriwat, N., Walsh, P. J., Osborn, D. L., Percival, C. J., Lin, J. M., Shallcross, D. E., Sheps, L., Klippenstein, S. J., Taatjes, C. A. and Lester, M. I. (2020) Direct kinetic measurements and theoretical predictions of an isoprene-derived Criegee intermediate. *Proc. Natl. Acad. Sci. U. S. A.* **117**, 9733–9740. https://doi.org/10.1073/pnas.1916711117.

8. Ting, A. W.-L. and Lin, J. J.-M. (2017) UV Spectrum of the Simplest Deuterated Criegee Intermediate CD2OO. *J. Chinese Chem. Soc.* **64**, 360–368. https://doi.org/10.1002/jccs.201700049.

9. Smith, M. C., Ting, W. L., Chang, C. H., Takahashi, K., Boering, K. A. and Lin, J. J. M. (2014) UV absorption spectrum of the C2 Criegee intermediate CH3CHOO. *J. Chem. Phys.* **141**, 074302. https://doi.org/10.1063/1.4892582.

10. Chang, Y.-P., Chang, C.-H., Takahashi, K. and Lin, J. J.-M. (2016) Absolute UV absorption cross sections of dimethyl substituted Criegee intermediate (CH3)2COO. *Chem. Phys. Lett.* **653**, 155–160. https://doi.org/https://doi.org/10.1016/j.cplett.2016.04.082.

11. Lin, Y.-H., Yin, C., Takahashi, K. and Lin, J. J.-M. (2021) Surprisingly long lifetime of methacrolein oxide, an isoprene derived Criegee intermediate, under humid conditions. *Commun. Chem.* **4**, 12. https://doi.org/10.1038/s42004-021-00451-z.

12. Vansco, M. F., Marchetti, B. and Lester, M. I. (2018) Electronic spectroscopy of methyl vinyl ketone oxide: A four-carbon unsaturated Criegee intermediate from isoprene ozonolysis. *J. Chem. Phys.* **149**, 244309. https://doi.org/10.1063/1.5064716.

13. Mir, Z. S., Lewis, T. R., Onel, L., Blitz, M. A., Seakins, P. W. and Stone, D. (2020) CH2OO Criegee intermediate UV absorption cross-sections and kinetics of CH2OO + CH2OO and CH2OO + I as a function of pressure. *Phys. Chem. Chem. Phys.* **22**, 9448–9459. https://doi.org/10.1039/d0cp00988a.

14. Foreman, E. S. and Murray, C. (2015) Kinetics of IO Production in the CH2I + O2 Reaction Studied by Cavity Ring-Down Spectroscopy. *J. Phys. Chem. A* **119**, 8981–8990. https://doi.org/10.1021/acs.jpca.5b05058.

15. Lin, Y.-H., Takahashi, K. and Lin, J. J.-M. (2022) Absolute photodissociation cross sections

of thermalized methyl vinyl ketone oxide and methacrolein oxide. *Phys. Chem. Chem. Phys.* https://doi.org/10.1039/D2CP00476C.

16. Sršeň, Hollas, D. and Slavíček, P. (2018) UV absorption of Criegee intermediates: Quantitative cross sections from high-level: Ab initio theory. *Phys. Chem. Chem. Phys.* **20**, 6421–6430. https://doi.org/10.1039/c8cp00199e.

17. Dawes, R., Jiang, B. and Guo, H. (2015) UV Absorption Spectrum and Photodissociation Channels of the Simplest Criegee Intermediate (CH2OO). *J. Am. Chem. Soc.* **137**, 50–53. https://doi.org/10.1021/ja510736d.

18. Aplincourt, P., Henon, E., Bohr, F. and Ruiz-López, M. F. (2002) Theoretical study of photochemical processes involving singlet excited states of formaldehyde carbonyl oxide in the atmosphere. *Chem. Phys.* **285**, 221–231. https://doi.org/10.1016/S0301-0104(02)00804-2.

19. Foreman, E. S., Kapnas, K. M., Jou, Y. T., Kalinowski, J., Feng, D., Gerber, R. B. and Murray, C. (2015) High resolution absolute absorption cross sections of the B1A′-X1A′ transition of the CH2OO biradical. *Phys. Chem. Chem. Phys.* **17**, 32539–32546. https://doi.org/10.1039/c5cp04977f.

20. McCoy, J. C., Marchetti, B., Thodika, M. and Karsili, T. N. V (2021) A Simple and Efficient Method for Simulating the Electronic Absorption Spectra of Criegee Intermediates: Benchmarking on CH2OO and CH3CHOO. *J. Phys. Chem. A*. https://doi.org/10.1021/acs.jpca.1c01074.

21. McCoy, J. C., Leger, S. J., Frey, C. F., Vansco, M. D., Marchetti, B. and Karsili, T. N. V. (2022) Modeling the Conformer-Dependent Electronic Absorption Spectra and Photolysis Rates of Methyl Vinyl Ketone Oxide and Methacrolein Oxide. *J. Phys. Chem. A* 10.1021/acs.jpca.1c08381. https://doi.org/10.1021/acs.jpca.1c08381.

22. Beames, J. M., Liu, F., Lu, L. and Lester, M. I. (2012) Ultraviolet Spectrum and Photochemistry of the Simplest Criegee Intermediate CH2OO. *J. Am. Chem. Soc.* **134**, 20045–20048. https://doi.org/10.1021/ja310603j.

23. Vansco, M. F., Marchetti, B., Trongsiriwat, N., Bhagde, T., Wang, G., Walsh, P. J., Klippenstein, S. J. and Lester, M. I. (2019) Synthesis, Electronic Spectroscopy, and Photochemistry of Methacrolein Oxide: A Four-Carbon Unsaturated Criegee Intermediate from Isoprene Ozonolysis. *J. Am. Chem. Soc.* **141**, 15058–15069. https://doi.org/10.1021/jacs.9b05193.

24. Karsili, T. N. V, Marchetti, B., Lester, M. I. and Ashfold, M. N. R. (2022) Electronic Absorption Spectroscopy and Photochemistry of Criegee Intermediates. *Photochem. Photobiol.* **n/a**. https://doi.org/https://doi.org/10.1111/php.13665.

25. Barber, V. P., Pandit, S., Green, A. M., Trongsiriwat, N., Walsh, P. J., Klippenstein, S. J. and Lester, M. I. (2018) Four-Carbon Criegee Intermediate from Isoprene Ozonolysis: Methyl Vinyl Ketone Oxide Synthesis, Infrared Spectrum, and OH Production. *J. Am. Chem. Soc.* **140**, 10866–10880. https://doi.org/10.1021/jacs.8b06010.

26. Hansen, A. S., Liu, Z., Chen, S., Schumer, M. G., Walsh, P. J. and Lester, M. I. (2020) Unraveling Conformer-Specific Sources of Hydroxyl Radical Production from an Isoprene-Derived Criegee Intermediate by Deuteration. *J. Phys. Chem. A* **124**, 4929–4938. https://doi.org/10.1021/acs.jpca.0c02867.

27. Caravan, R. L., Vansco, M. F., Au, K., Khan, M. A. H., Li, Y.-L., Winiberg, F. A. F., Zuraski, K., Lin, Y.-H., Chao, W., Trongsiriwat, N., Walsh, P. J., Osborn, D. L., Percival, C. J., Lin, J. J.-M., Shallcross, D. E., Sheps, L., Klippenstein, S. J., Taatjes, C. A. and Lester, M. I. (2020) Direct kinetic measurements and theoretical predictions of an isoprene-derived Criegee

intermediate. *Proc. Natl. Acad. Sci.* **117**, 9733 LP – 9740. https://doi.org/10.1073/pnas.1916711117.

28. Vansco, M. F., Caravan, R. L., Zuraski, K., Winiberg, F. A. F., Au, K., Trongsiriwat, N., Walsh, P. J., Osborn, D. L., Percival, C. J., Khan, M. A. H., Shallcross, D. E., Taatjes, C. A. and Lester, M. I. (2020) Experimental Evidence of Dioxole Unimolecular Decay Pathway for Isoprene-Derived Criegee Intermediates. *J. Phys. Chem. A* **124**, 3542–3554. https://doi.org/10.1021/acs.jpca.0c02138.

29. Vansco, M. F., Zuraski, K., Winiberg, F. A. F., Au, K., Trongsiriwat, N., Walsh, P. J., Osborn, D. L., Percival, C. J., Klippenstein, S. J., Taatjes, C. A., Lester, M. I. and Caravan, R. L. (2021) Functionalized Hydroperoxide Formation from the Reaction of Methacrolein-Oxide, an Isoprene-Derived Criegee Intermediate, with Formic Acid: Experiment and Theory. *Molecules* **26**. https://doi.org/10.3390/molecules26103058.

30. Esposito, V. J., Tianlin, L., Wang, G., Caracciolo, A., Vansco, M. F., Marchetti, B., Karsili, T. N. V. and Lester, M. I. (2021) Photodissociation Dynamics of CH2OO on Multiple Potential Energy Surfaces: Experiment and Theory. *J. Phys. Chem. A*. https://doi.org/10.1021/acs.jpca.1c03643.

31. Wang, G., Liu, T., Caracciolo, A., Vansco, M. F., Trongsiriwat, N., Walsh, P. J., Marchetti, B., Karsili, T. N. V and Lester, M. I. (2021) Photodissociation dynamics of methyl vinyl ketone oxide: A four-carbon unsaturated Criegee intermediate from isoprene ozonolysis. *J. Chem. Phys.* **155**, 174305. https://doi.org/10.1063/5.0068664.

32. Antwi, E., Bush, R., Marchetti, B. and Karsili, T. (2022) A direct dynamics study of the exotic photochemistry of the simplest Criegee intermediate, CH2OO. *Phys. Chem. Chem. Phys.* **24**, 16724–16731. https://doi.org/10.1039/d2cp01860h.

33. Caravan, R. L., Vansco, M. F., Au, K., Khan, A. A. H., Li, Y.-L. L., Winiberg, F. A. F. F., Zuraski, K., Lin, Y.-H. H., Chao, W., Trongsiriwat, N., Walsh, P. J., Osborn, D. L., Percival, C. J., Lin, J. J.-M. M., Shallcross, D. E., Sheps, L., Klippenstein, S. J., Taatjes, C. A., Lester, M. I., Khan, M. A. H., Li, Y.-L. L., Winiberg, F. A. F. F., Zuraski, K., Lin, Y.-H. H., Chao, W., Trongsiriwat, N., Walsh, P. J., Osborn, D. L., Percival, C. J., Lin, J. J.-M. M., Shallcross, D. E., Sheps, L., Klippenstein, S. J., Taatjes, C. A. and Lester, M. I. (2020) Direct kinetic measurements and theoretical predictions of an isoprene-derived Criegee intermediate. *Proc. Natl. Acad. Sci.* **117**, 9733 LP – 9740. https://doi.org/10.1073/pnas.1916711117.

34. Lin, Y. H., Takahashi, K. and Lin, J. J. M. (2022) Absolute photodissociation cross sections of thermalized methyl vinyl ketone oxide and methacrolein oxide. *Phys. Chem. Chem. Phys.* **24**, 10439–10450. https://doi.org/10.1039/d2cp00476c.

35. Zhong, J., Kumar, M., Zhu, C. Q., Francisco, J. S. and Zeng, X. C. (2017) Surprising Stability of Larger Criegee Intermediates on Aqueous Interfaces. *Angew. Chemie Int. Ed.* **56**, 7740–7744. https://doi.org/10.1002/anie.201702722.

36. Lin, Y. H., Yin, C., Takahashi, K. and Lin, J. J. M. (2021) Surprisingly long lifetime of methacrolein oxide, an isoprene derived Criegee intermediate, under humid conditions. *Commun. Chem.* **4**, 1–20. https://doi.org/10.1038/s42004-021-00451-z.

37. Esposito, V. J., Werba, O., Bush, S. A., Marchetti, B. and Karsili, T. N. V (2021) Insights into the Ultrafast Dynamics of CH2OO and CH3CHOO Following Excitation to the Bright 1ππ* State: The Role of Singlet and Triplet States. *Photochem. Photobiol.* **n/a**. https://doi.org/https://doi.org/10.1111/php.13560.

38. Grimme, S. (2006) Semiempirical hybrid density functional with perturbative second-order correlation. *J. Chem. Phys.* **124**, 34108. https://doi.org/10.1063/1.2148954.

39. Dunning, T. H. (1989) Gaussian basis sets for use in correlated molecular calculations. I. The atoms boron through neon and hydrogen. *J. Chem. Phys.* **90**, 1007–1023. https://doi.org/10.1063/1.456153.

40. Antwi, E., Bush, R., Marchetti, B. and Karsili, T. (2022) Climbing up Conical Intersections: A Direct Dynamics Study of the Exotic Photochemistry of Criegee Intermediates. *Phys. Chem. Chem. Phys.* https://doi.org/10.1039/D2CP01860H.

41. Barbatti, M., Granucci, G., Persico, M., Ruckenbauer, M., Vazdar, M., Eckert-Maksić, M. and Lischka, H. (2007) The on-the-fly surface-hopping program system Newton-X: Application to ab initio simulation of the nonadiabatic photodynamics of benchmark systems. *J. Photochem. Photobiol. A Chem.* **190**, 228–240. https://doi.org/https://doi.org/10.1016/j.jphotochem.2006.12.008.

42. Barbatti, M., Ruckenbauer, M., Plasser, F., Pittner, J., Granucci, G., Persico, M. and Lischka, H. (2013) Newton-X: a surface-hopping program for nonadiabatic molecular dynamics. *Wiley Interdiscip. Rev. Comput. Mol. Sci.* **4**, 26–33. https://doi.org/doi:10.1002/wcms.1158.

43. Butcher, J. C. (1965) A Modified Multistep Method for the Numerical Integration of Ordinary Differential Equations. *J. ACM* **12**, 124–135. https://doi.org/10.1145/321250.321261.

44. Park, J. W. and Shiozaki, T. (2017) Analytical Derivative Coupling for Multistate CASPT2 Theory. *J. Chem. Theory Comput.* **13**. https://doi.org/10.1021/acs.jctc.7b00018.

45. Shiozaki, T. (2018) BAGEL: Brilliantly Advanced General Electronic-structure Library. *WIREs Comput. Mol. Sci.* **8**, e1331. https://doi.org/10.1002/wcms.1331.

46. Werner, H.-J., Knowles, P. J., Knizia, G., Manby, F. R., Schütz, M., Celani, P., Györffy, W., Kats, D., Korona, T., Lindh, R., Mitrushenkov, A., Rauhut, G., Shamasundar, K. R., Adler, T. B., Amos, R. D., Bennie, S., Bernhardsson, A., Berning, A., Cooper, D. L., Deegan, M. J. O.,

Dobbyn, A. J., Eckert, F., Goll, E., Hampel, C., Hesselmann, A., Hetzer, G., Hrenar, T., Jansen, G., Köppl, C., Lee, S. J. R., Liu, Y., Lloyd, A. W., Ma, Q., Mata, R. A., May, A. J., McNicholas, S. J., Meyer, W., III, T. F. M., Mura, M. E., Nicklass, A., O'Neill, D. P., Palmieri, P., Peng, D., Pflüger, K., Pitzer, R., Reiher, M., Shiozaki, T., Stoll, H., Stone, A. J., Tarroni, R., Thorsteinsson, T., Wang, M. and Welborn, M. (2018) MOLPRO, version 2018.1, a package of ab initio programs.

47. Werner, H.-J., Knowles, P. J., Knizia, G., Manby, F. R. and Schütz, M. (2012) Molpro: a general-purpose quantum chemistry program package. *WIREs Comput. Mol. Sci.* **2**, 242–253. https://doi.org/10.1002/wcms.82.

48. , M. J. Frisch, G. W. Trucks, H. B. Schlegel, G. E. Scuseria, M. A. Robb, J. R. Cheeseman, G. Scalmani, V. Barone, G. A. Petersson, H. Nakatsuji, X. Li, M. Caricato, A. V. Marenich, J. Bloino, B. G. Janesko, R. Gomperts, B. Mennucci, H. P. Hratchian, J. V,  and D. J. F. (2016) Gaussian 16, Revision C.01. *Gaussian Inc. Wallingford CT*.